PROCEEDINGS OF SCIENCE

Birefringence: Effects and Implications for In-Ice Radio Detection of Neutrinos

Nils Heyer[a,*] **and Christian Glaser**[a]

[a] *Uppsala University Department of Physics and Astronomy, Uppsala, SE-752 37, Sweden*

E-mail: nils.heyer@physics.uu.se, christian.glaser@physics.uu.se

The detection of high-energy neutrinos in the EeV range requires new detection techniques to cope with the small expected flux. The radio detection method, utilizing Askaryan emission, can be used to detect these neutrinos in polar ice. The propagation of the radio pulses has to be modeled carefully to reconstruct the energy, direction, and flavor of the neutrino from the detected radio flashes. Here, we study the effect of birefringence in ice, which splits up the radio pulse in two orthogonal polarization components with slightly different propagation speeds. This provides useful signatures to determine the neutrino energy and is potentially important to determine the neutrino direction to degree precision. We calculated the effect of birefringence from first principles where the only free parameter is the dielectric tensor as a function of position. Our code can propagate full RF waveforms which for the first time allows taking interference due to changing polarization eigenvectors during propagation into account. The model is available open-source through the NuRadioMC framework. We compare our results to in-situ calibration data from the ARA and ARIANNA experiments and find good agreement for the available time delay measurements, improving the predictions significantly compared to previous studies. Finally, the implications and opportunities for neutrino detection are discussed. The results presented here are based on the publication Ref. [1].

9th International Workshop on Acoustic and Radio EeV Neutrino Detection Activities - ARENA2022
7-10 June 2022
Santiago de Compostela, Spain

*Speaker

PoS(ARENA2022)021

1. Introduction

The in-ice radio detection of cosmic neutrinos is a promising approach to measuring the first neutrinos in the EeV range. In order to do so, a large volume of ice has to be instrumented with radio antennas close to the surface of the ice sheet. When a high-energy neutrino interacts in the polar ice, the resulting particle shower emits coherent radio pulses via the Askarian effect. These pulses can potentially traverse a few kilometers of ice until reaching an antenna. To understand the measured radio pulses, the effects the ice has on the propagation have to be modeled precisely.

1.1 Birefringence

Birefringence is a material property of the glacial ice at the South Pole, which is defined by a dependency of the refractive index on the polarization and direction of the propagating wave. This can lead to a time delay and amplitude modulation between different measured polarization states. It can affect the energy as well as the direction reconstruction and the estimation of the effective volume of the experiments. Many ice-related effects are already accounted for in the MC simulations used for the in-ice radio detection of neutrinos. Those include attenuation, a bending of the propagation path due to a changing density, or reflective ash layers that can reflect parts of the radio signal. For this study of birefringence, the ice of the South Pole is considered a continuous medium with slightly changing refractive indices for different directions and depths. This effect is mainly due to the crystal structure of the ice and the horizontal pressure due to glacial flow. Overshadowing the birefringence effect is a depth-dependent density effect that changes the refractive index significantly.

1.2 Theoretical Foundation

The birefringence effect can be derived from the solutions to Maxwells' equations for plane waves. Effectively, an electromagnetic wave traveling through a birefringent medium splits into two distinct eigenstates which can be characterized by their effective refractive index and their polarization eigenvector. All that is needed to calculate these properties are the propagation direction $\vec{s} = (s_x,\ s_y,\ s_z)$ and the dielectric tensor, which diagonalizes in the correct basis and can be parametrized through three refractive indices n_x, n_y and n_z. The basis which diagonalizes the dielectric tensor is defined such that the z-axis points in the vertical direction, the x-axis points parallel to the ice flow, and the y-axis points perpendicular to the ice flow. The derivation from Maxwells' equations results in Eq. (1). Solving this equation for n (which can be done analytically), results in two unique solutions which are the effective refractive indices $N_{1/2}$. The calculation for the polarization eigenvectors $\vec{e}_i$ follows from Eq. (2). When $N_i = n_x,\ n_y\ or\ n_z$ special cases have to be introduced to calculate the polarization eigenvectors. As the propagation direction can be calculated from a ray tracing algorithm (analytical or numerical) which is also defined by the ice properties, the only free parameter is the dielectric tensor modeling the ice. This derivation was taken from Ref. [2].

$$\begin{aligned}&\left(n_x^2 - n^2\right)\left(n_y^2 - n^2\right)\left(n_z^2 - n^2\right)\\ &+ n^2\left[s_x^2\left(n_y^2 - n^2\right)\left(n_z^2 - n^2\right) + s_y^2\left(n_x^2 - n^2\right)\left(n_z^2 - n^2\right) + s_z^2\left(n_x^2 - n^2\right)\left(n_y^2 - n^2\right)\right] = 0\end{aligned} \tag{1}$$

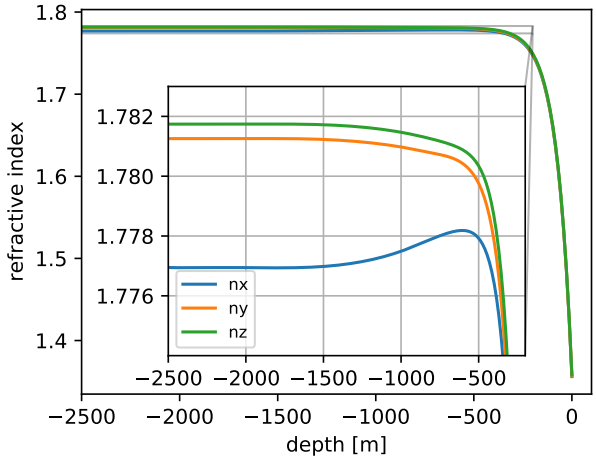

Figure 1: Refractive index as a function of depth. Combination of birefringence and density effects. The zoomed-in version highlights the birefringence effects seen in Fig. 1 while the zoomed-out version highlights the density effects. The figure and the caption were taken from Ref. [1].

$$\vec{e}_i = \left(\frac{s_x}{N_i^2 - n_x^2}, \quad \frac{s_y}{N_i^2 - n_y^2}, \quad \frac{s_z}{N_i^2 - n_z^2} \right) \tag{2}$$

1.3 Ice Model

The measurement of the dielectric properties of polar ice was performed in the SPIce borehole and the data is available at Ref. [3]. The calculations to convert the dielectric data into refractive indices were taken from Ref. [4]. The data was interpolated via a spline fit and extrapolated to more shallow and deeper depths. As this data did not take any density effects into account, these effects were added to the interpolated functions for the three refractive indices. In the following, an exponential parametrization of the density effect was used for the simulation. The result can be seen in Fig. 1. It shows that on a large scale the density effect dominates as the refractive indices change from ~ 1.3 at shallow depths to ~ 1.78 at deeper depths. However, when zooming into the plot one can see the differences in refractive indices due to birefringence.

2. Pulse Propagation

When calculating and analyzing the behavior of the effective refractive indices and polarization eigenvectors for different emitter-antenna geometries, we find that, especially for a propagation direction parallel to the ice flow, the values change drastically at different stages of the propagation (see Fig. 5 left). However, a changing polarization means that the two eigenstates mix during propagation. These changes have to be accounted for to calculate the effects of birefringence on the pulse shapes properly. The algorithm used to track these changes takes the electric field at the point of emission and then incrementally propagates the pulse through the ice according to the effective refractive indices and polarization eigenstates at the incremental step of the propagation. We rotate the electric field, according to the polarization eigenvectors into the basis in which the pulses travel

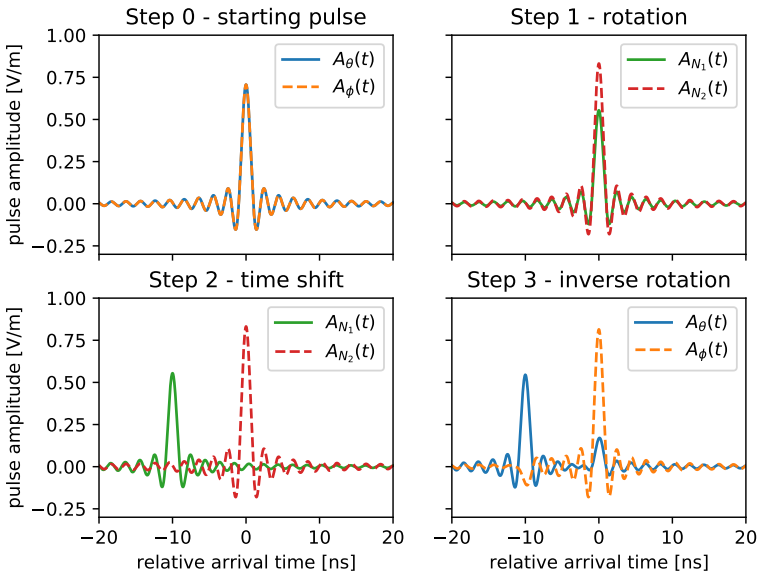

Figure 2: Numerical pulse modulation for an incremental step in the propagation calculation for an artificial pulse shape. The figure was taken from Ref. [1].

at different velocities due to the effective refractive indices (step 1), apply the appropriate time shift for the traversed incremental step (step 2), and finally rotate back into the original basis using the inverse of the previously defined rotation matrix (step 3). The rotation matrix and the three steps of the propagation are further illustrated in the equations Eq. (3), (4), (5), (6) as well as in Fig. 2.

$$R = \begin{pmatrix} e_\perp^r & e_\perp^\theta & e_\perp^\phi \\ e_1^r & e_1^\theta & e_1^\phi \\ e_2^r & e_2^\theta & e_2^\phi \end{pmatrix} \approx \begin{pmatrix} 1 & 0 & 0 \\ 0 & e_1^\theta & e_1^\phi \\ 0 & e_2^\theta & e_2^\phi \end{pmatrix} \tag{3}$$

$$\begin{pmatrix} A_{N_1}(t) \\ A_{N_2}(t) \end{pmatrix} = R \begin{pmatrix} A_\theta(t) \\ A_\phi(t) \end{pmatrix} \tag{4}$$

$$A_{N_1}(t) \longrightarrow A_{N_1}(t - \Delta t) \tag{5}$$

$$\begin{pmatrix} A_\theta(t) \\ A_\phi(t) \end{pmatrix} = R^{-1} \begin{pmatrix} A_{N_1}(t) \\ A_{N_2}(t) \end{pmatrix} \tag{6}$$

3. Comparison of model predictions and experimental measurements

To test the predictions of the introduced birefringence calculations, the time delay and polarization/amplitude predictions were compared to measurements made by the ARA and ARIANNA collaboration. These measurements were performed by lowering a radio emitter into the SPIce hole to calibrate the antennas for radio signals emitted at different depths. The emitted pulses propagated

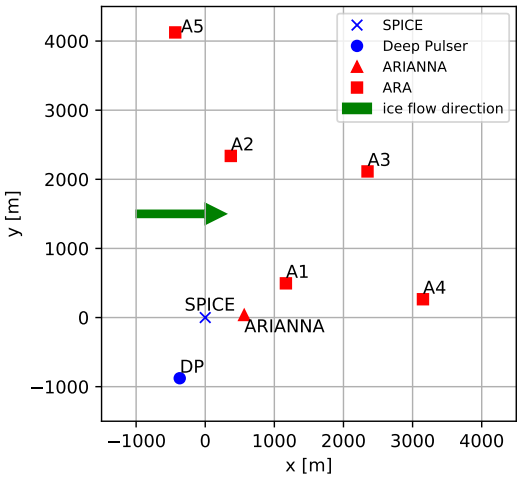

Figure 3: The geometry of the measurement setup at the South Pole Ref. [5], with the SPIce hole for the transmitter in blue and the ARA and ARIANNA antenna stations in red. Also shown is the position of the *deep pulser* (Ref. [4]), another radio transmitter attached to the end of one of the IceCube strings. The figure and the caption were taken from Ref. [1].

through the ice and were picked up by different antenna stations such that the direction of the propagation path had a different angle to the ice flow for different stations. From the waveforms, the fluence, polarization, and the time delay were extracted. The fluence $f_{\theta,\phi}$ is a measure of how much energy is stored in the electric field $E_{\theta,\phi}$ of a pulse by integrating over a time window of ±35 ns around the maximum of the Hilbert envelope. To measure it Eq. 7 was used.

$$f_{\theta,\phi} = \sqrt{\sum_{t=t_m-35ns}^{t_m+35ns} |E_{\theta,\phi}(t)|^2 - f_{\theta,\phi,noise}} \tag{7}$$

The polarization of the pulse is the ratio of the fluence between the ϕ and the θ component. The time delay between the θ and ϕ components was calculated with a subtraction between the two maxima of the Hilbert envelopes of the respective pulse components.

3.1 Experimental Setup

An overview of the emitter and receiver sites can be seen in Fig. 3. As the distance between the emitter and the antennas differs greatly the launch angles at which the pulses are sent out also differ. As previous measurements in an anechoic chamber have shown, the initial polarization of the emitted pulses depends on the launch angle (Ref. [6]), which we account for in the simulations. The emitter used for the measurements has also been characterized in an anechoic chamber and the resulting pulse traces have been used for the presented analysis (Ref. [6]). In these measurements fluctuations in the data already showed a time offset between the θ and ϕ components, as well as a phi component very close to the noise level for many launch angles. Our birefringence calculations allow for the first time to take these observations into account.

	simple calculation		pulse propagation		measured data
	$\boldsymbol{\Delta T_{\theta,\phi}}$ **[ns]** (this work)	$\Delta T_{\theta,\phi}$ [ns] (Ref. [4])	$\boldsymbol{\Delta T_{\theta,\phi}}$ **[ns]** (this work)	$\boldsymbol{\Delta T_{v,h}}$ **[ns]** (this work)	$\Delta T_{v,h}$ [ns] (ARA [4])
SPIce - A2	**−21.7**	−22.5	**−11.6 ± 0.7**	**−10.9 ± 0.4**	−14.1 ± 2.8
SPIce - A4	**−5.5**	−1.6	**4.1 ± 1.1**	**3.9 ± 0.2**	4.6 ± 9

Table 1: Summary of time delay measurements and predictions for the pulse propagation from 1000 m depth to the ARA A2 and A4 stations. The first two columns show the accumulated time delay in the θ and ϕ polarization components using a simplified birefringence model. The third/fourth columns show the time delay extracted from the propagated waveforms of the electric field (θ, ϕ) and include the antenna response (v, h). The last column shows the measured time delay between the vpol and hpol antennas. See text for details. The values indicated in bold fond represent our predictions and the normal fond values represent the predictions and measurements published in Ref. [4]. The table and the caption were taken from Ref. [1].

3.2 Time Delay

Using the SPIce emitter as well as a second emitter called 'Deep Pulser' at positions indicated in Fig. 3, radio pulses were sent from different depths and the time delay between the θ and ϕ component was measured at different antenna stations. A previously used birefringence model presented in Ref. [4], predicted these time delays as a function of depths. However, none of the calculated time delays take the systematic time difference at the emitter into account. When performing a pulse propagation for the pulses measured in the anechoic chamber emitted from the SPIce emitter, the predicted time difference changes significantly (depending on the geometry this can be more than 10 ns, see Tab. 1). Comparing the two available measured data points for the time delay with the propagated pulse prediction shows good agreement within a 1-sigma limit. A comparison of the different birefringence models and the more precise pulse propagation for the two data points can be seen in Tab. 1.

3.3 Amplitude Modulation

Additionally to the time delay measurements, emitter depth-dependent amplitude measurements were published by ARA, and emitter depth-dependent polarization measurements were published by ARIANNA. Depending on the depth of the emitter, the amplitude/polarization of the measured pulses showed an oscillatory behavior. It was hypothesized that this effect was due to birefringence. To test this hypothesis the pulses measured in the anechoic chamber were propagated for these geometries and the amplitude/polarization of the resulting waveforms was compared to the measured data. As an example of this process, the comparison to the ARIANNA measurements is presented in Fig. 4. We find that birefringence does not change the amplitude/polarization for these geometries in a significant way.

3.4 Impact on Neutrino Detection

The detection of neutrinos via the radio technique requires high precision when it comes to measuring the timing and polarization of the radio pulses. Any mechanism that influences these parameters will inevitably have an impact on the detection process. For example, a changing signal

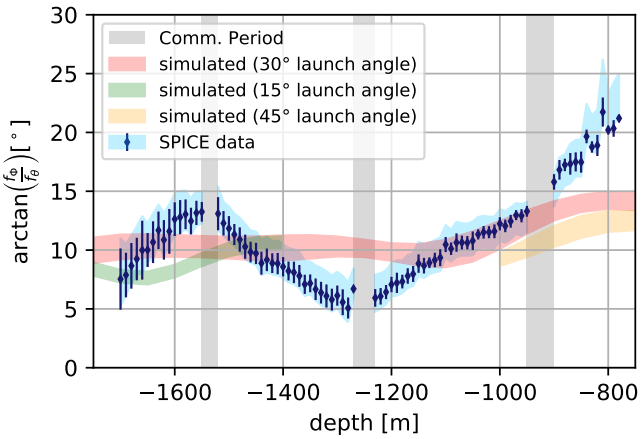

Figure 4: Measured polarization at the ARIANNA station and the expected polarization after propagating the anechoic chamber pulses through the birefringence model. The adjacent launch angles of 15 and 45 degrees were included for comparison. The gray areas mark communication periods during which no data was taken. The SPIce data was averaged over 10 m depths, and the 1σ spread of the distribution is shown with the blue error bars. The light blue shading indicates the systematic uncertainty on the reconstruction stemming from systematic uncertainties in the ARIANNA LPDA orientations (see Ref. [6] for details). The figure and the caption were taken from Ref. [1].

shape could result in a lower amplitude and therefore the event could miss a voltage trigger, thus affecting the number of events detected and therefore the effective volume of the detector. It would also affect the ability to reconstruct the direction and energy of the initial neutrino from the measured radio pulses as those parameters also depend on the polarization and amplitude. However, the effect of birefringence also gives a handle on the distance from the neutrino interaction to the antenna as the measured time difference accumulates over distance and is thus correlated to the full path length. As a first example of the change birefringence could cause, a neutrino-induced radio pulse was simulated using NuRadioMC and propagated through the birefringence model for a specific geometry. The changing polarization and the pulse expected to arrive at the antenna can be seen in Fig. 5. A further study is planned to investigate this question on the full impact of birefringence on neutrino detection via the radio method. However, we expect that the birefringence effect can be disentangled for most geometries.

4. Conclusion

Birefringence is an optical effect of a medium that, historically, has been well documented and mathematically described. Its effects on the detection of neutrinos using radio pulses have now been described in sufficient detail for the first time. The introduced calculations build on the mathematical foundation of Maxwells' equations and account for the inhomogeneities of the polar ice sheet. The ice model incorporates the most recent data from the South Pole but is flexible enough to work with arbitrary ice data, in case new data is taken or new locations are planned to be investigated. The propagation calculation extends the insight into the effects of birefringence by allowing to propagate arbitrary pulse forms for arbitrary geometries. The simulation code was

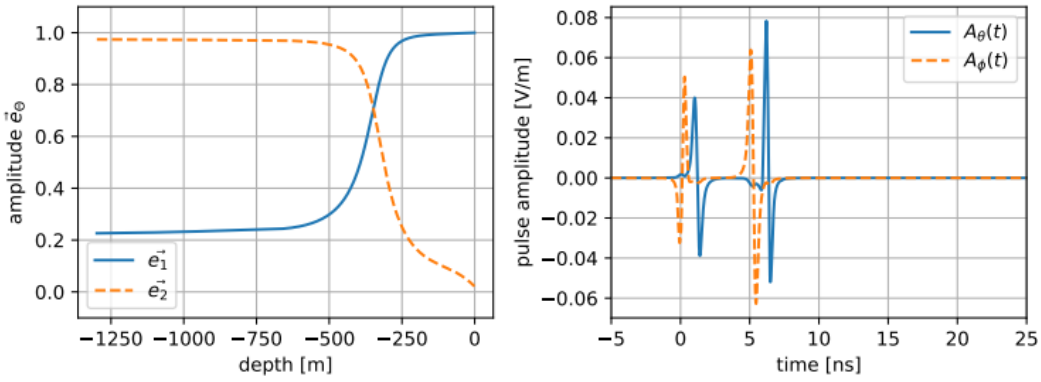

Figure 5: A typical pulse shape generated from NuRadioMC and propagated through the introduced birefringence model. The left side shows the polarization of the two propagating states against the depth. The right side shows the expected traces after propagating from to the given antenna positions. The position of the neutrinos source was set to [0 m, 0 m, −1300 m] and the antenna was set to [1487 m, 200 m, −1 m]. The figure and the caption were adapted from Ref. [1].

included in the NuRadioMC framework (Ref. [7]). Applying the birefringence calculations to real emitter-antenna geometries and comparing the results to measured data indicates that the time delay caused by birefringence is a measurable effect that can be simulated in the described manner. It further suggests that the depth-dependent oscillations measured by ARA and ARIANNA are not due to birefringence. Further investigations are needed to quantify the impact of birefringence on the effective volume and direction/energy reconstruction capabilities of an in-ice radio detector.

References

[1] N. Heyer and C. Glaser, *First-principle calculation of birefringence effects for in-ice radio detection of neutrinos*, arXiv:2205.06169.

[2] P. Kužel, *Electromagnétisme des milieux continus*, *Université Paris-Nord: Institut Galilée,* https://www.fzu.cz/~kuzelp/Optics/Optique.pdf (2001) 82–88.

[3] D. E. Voigt, *c-Axis Fabric of the South Pole Ice Core, SPC14*, *U.S. Antarctic Program (USAP) Data Center* (2017) .

[4] T. M. Jordan et al., *Modeling ice birefringence and oblique radio wave propagation for neutrino detection at the South Pole*, *Annals of Glaciology* **61** (2020) 84–91.

[5] A. Connolly, *Impact of biaxial birefringence in polar ice at radio frequencies on signal polarizations in ultra-high energy neutrino detection*, arXiv:2110.09015.

[6] ARIANNA collaboration, A. Anker et al., *Probing the angular and polarization reconstruction of the ARIANNA detector at the South Pole*, *Journal of Instrumentation* **15** (2020) P09039–P09039.

[7] C. Glaser et al., *NuRadioMC: Simulating the radio emission of neutrinos from interaction to detector*, *EPJ* **C80** (2020) 77.